Bol. Soc. Paran. Mat.
©SPM – E-ISSN-2175-1188
SPM: www.spm.uem.br/bspm

(3s.) **v. 2025 (43) 2** : 1–16.
ISSN-0037-8712
doi:10.5269/bspm.78807

# Pattern Formation in Bazykina's Predator-Prey Model with Holling Type-III Response: A Multiscale Perturbation Analysis

Atish Kumar Sethy and Jyotiska Datta*

ABSTRACT: The dynamics of interacting populations—such as rival species or predator-prey systems—can be more thoroughly understood through the study of spatiotemporal pattern formation. Reaction-diffusion systems are commonly used to model such interactions. These models exhibit a wide range of well-known patterns, including travelling waves, periodic travelling waves, spots, labyrinthine structures, mixed spot-stripe patterns, spatiotemporal chaos, and interacting spiral chaos. Under appropriate parametric conditions, both target and spiral wave patterns can emerge. Notably, spiral patterns have been observed to evolve at the Turing-Hopf threshold; however, the precise formalism responsible for their emergence has remained unclear. This study employs a multiscale perturbation analysis to elucidate the mechanisms behind spiral pattern formation under suitable parametric regimes. A key contribution of this work is the discovery that spiral patterns can be generated by initiating numerical simulations from approximate analytical solutions. The behavioral insights derived from this study are broadly applicable to a wide class of pattern-forming systems that exhibit spiral structures, as well as to general spatiotemporal models of interacting populations.

Key Words: Turing patterns, Hopf bifurcation, spatial pattern, linear amplitude equation.

## Contents



## 1. Introduction

Turing's groundbreaking work [39] has been fundamental in advancing scientific understanding of pattern formation mechanisms across a wide range of physical, chemical, and biological systems. These include physical processes such as ripple formation in sand and river meandering; chemical processes like the FitzHugh–Nagumo reaction and the Belousov–Zhabotinsky reaction; and biological processes such as vegetation pattern formation, morphogenesis, and the emergence of animal skin patterns [13,33]. A common mathematical framework for describing these phenomena involves reaction-diffusion equations, extensively explored by Murray in his studies of spatiotemporal pattern formation [33]. Turing instability—a diffusion-driven mechanism—occurs when a spatially uniform equilibrium becomes unstable, giving rise to stable, stationary Turing patterns. Moreover, the interaction between Hopf bifurcations

* Coresponding author.
2010 *Mathematics Subject Classification:* 35B36, 35K57, 37H20.
Submitted September 06, 2025. Published September 30, 2025

(which induce temporal oscillations) and Turing instabilities (which induce spatial structures) can lead to complex spatiotemporal behaviors near the so-called Turing–Hopf bifurcation point [3]. Among the diverse patterns that emerge from such systems, spiral and target patterns have been recognized as distinct classes that cannot be fully explained by classical Turing mechanisms alone. Spiral patterns typically arise in parameter regimes with low diffusivity near the Hopf bifurcation boundary, where oscillatory kinetics dominate. Tyson et al. [41] identified two hallmark periodic patterns in two-dimensional media: rotating spiral waves and outward-propagating concentric waves, referred to as target patterns. When a target wave is perturbed locally, it can deform and give rise to spiral waves—a phenomenon also described by Riaz [35]. Ghosh and Ray [17] further characterized target patterns as broader extensions of spiral wave structures, emphasizing their interconnected nature in reaction-diffusion systems.

Spatiotemporal patterns such as spinning spiral waves and concentric circular target waves were first observed in demonstrations of the Belousov–Zhabotinsky (BZ) reaction, where spiral waves emanate from a core and target patterns arise as concentric wavefronts [46,49]. Kopell and Howard [25] identified both target patterns and spiral waves in certain classes of nonlinear reaction–diffusion equations, highlighting their mathematical foundation. Experimentally, the formation of target patterns has often been associated with spatial heterogeneities at their centers. Examples include minor inhomogeneities in the BZ reagents and periodic activation by oscillatory cells in the heart ventricle [40]. Spiral wave patterns have also been observed in biological contexts such as cardiac arrhythmias [18], where spiral dynamics contribute to irregular heart rhythms, and in the aggregation phase of slime moulds, where communication occurs via traveling waves of cyclic adenosine monophosphate (cAMP) [42]. Further experimental studies have explored the formation of multi-armed spiral patterns [38], while analytical investigations have examined the mechanism by which a single-armed spiral can split into multiple arms [34].

Significant contributions to the study of spiral and target pattern formation have been made by Kuramoto and collaborators. Their analytical investigations primarily employed the $\lambda - \omega$ system as a simplified model for capturing the essential dynamics of such patterns [26,27]. Using center manifold theory and the standard form technique, it is possible to derive a $\lambda - \omega$ system from the temporal component of any spatiotemporal model near the Hopf bifurcation threshold [28]. Kuramoto and Yamada introduced a non-perturbative method for extracting spiral wave solutions from the $\lambda - \omega$ framework [47], while subsequent validation through numerical simulations was carried out by Kuramoto and Koga [26]. In addition, Kuramoto and Yamada provided a perturbative analysis of spiral and target solutions derived from the $\lambda - \omega$ system [27]. The presence of spiral patterns in reaction–diffusion models was further demonstrated numerically by Cohen et al. [12], supporting the theoretical predictions of the $\lambda - \omega$ approach.

Using a multiscale perturbation technique, Duffy and Greenberg were among the first to derive asymptotic first-order spiral wave solutions for $\lambda - \omega$ reaction–diffusion systems in 1980 [14,20]. Subsequently, Hagan [22,23] and Biktasheva [9] applied similar multiscale perturbation approaches directly to reaction–diffusion systems, bypassing the reduction to $\lambda - \omega$ form. Barkley and Kevrekidis [2] explored the influence of bifurcating eigenmodes on the spatiotemporal characteristics of spiral instabilities through linear stability analysis. The dynamics of systems near a bifurcation threshold are often described using amplitude equations [13,18]. These equations are particularly useful for understanding the emergence of spiral and target patterns, which typically appear close to the Hopf bifurcation curve or threshold. Several studies have combined theoretical development with numerical validation, as reported in various publications [15,16,17,35].

Numerical simulations have also been extensively used to study spiral and target pattern formation. For instance, in the Belousov–Zhabotinsky reaction–diffusion system, simulations have shown that reagent concentration plays a critical role in the formation of target patterns [10]. Gong et al. introduced a theoretical and computational framework for generating antispiral waves near the Hopf bifurcation boundary. Further numerical studies of spiral waves, particularly in the context of cardiac arrhythmias, are detailed in [1,11]. Zaritski et al. [48] investigated the numerical construction of multi-armed spirals in two-component Oregonator and FitzHugh–Nagumo-type models, providing additional insight into the mechanisms behind complex pattern formation.

Greenberg and Duffy et al. solved a set of $\lambda - \omega$ reaction-diffusion equations [14,20] using a multiscale perturbation technique, yielding first-order asymptotic spiral wave solutions. Biktasheva [9] and Hagan [22,23] employed a multiscale perturbation technique in place of converting the $\lambda - \omega$ system as opposed

to the reaction-diffusion systems. Barkley and Kevrekidis used linear stability analysis to investigate how bifurcating eigenmodes affect the spatiotemporal character of spiral instability [2]. Intensity equations [13,18] can describe a system's dynamics near a bifurcation threshold. Understanding the mechanism behind the creation of spirals and targets is aided by the associated amplitude equation, as these features are typically observed as close to the threshold or the Hopf bifurcation curve. Numerous papers contain such works in addition to numerical validation [15,16,17,35]. Exploring spiral and target pattern formation has also been done through numerical simulations. Numerical simulations by Bugrim et al. [10] demonstrated that the reagent concentration is the primary factor influencing the development of the Belousov-Zhabotinsky reaction-diffusion system's target pattern. The analytical and numerical theory for producing antispiral waves close to the Hopf-bifurcation border has been offered by Gong et al. [19]. Numerical approaches for spiral waves linked with cardiac arrhythmias have been thoroughly explored by Aslanidi et al. [1]. In their paper [48], Zaritski et al. examine the mathematical building of multiarmed spirals for two-component Oregonator models and FitzHugh-Nagumo type models.

Prey-predator interactions, described as a model of response equations for diffusion, are the main focus of investigations into Turing pattern development in diverse ecological systems. Turing patterns include mixtures of spots and stripes, labyrinthines, hot spots, cold spots, and non-stationary chaotic patterns [4,6,43]. The interacting chaotic spiral patterns that emerge at parameter values far from the Hopf threshold have been studied by Banerjee and Petrovskii [5] within the Turing-Hopf domain. From an ecological standpoint, spiral and target patterns can provide essential insights into the dynamics of coexisting populations and prey-predator interactions. Gurney and colleagues [21] have explained the generation of patterns such as spirals and circles in a spatial Rosenzweig-McArthur model. They propose that oscillations result from one species' invasion of another, which causes these patterns. Medvinsky et al. [32] have provided a numerical explanation for forming spirals from appropriate initial conditions that eventually collapse into a model of spatiotemporal chaos of the interaction between plankton and fish. Similar experiments have been conducted by Wang et al. [44,45] for the prey-predator system with functional responses of the Michaelis-Menten and Ivlev types. Circular (target-like) patterns are observed in a two-patch Rosenwig McArthur spatial model, according to Li et al [29]. When prey avoidance and predator pursuit are included, these circular waves subsequently disintegrate into spatiotemporal chaos [29]. Sheratt et al. provided evidence on how obstacles, like topography and size, impact target patterns [36,37].

This paper explores the possibility of spirals growing further or transforming into a deformed shape when they arise near the Hopf bifurcation border. We analyze the parameter values around the Hopf bifurcation border, where a stationary spiral is seen. It is demonstrated that choosing the right initial condition is just as crucial to producing the right patterns. We explain the formation of spirals and target patterns and validate the analytical results with numerical simulations. Additionally, we derive the diffusion's linear amplitude equation using Bazykin's prey-predator model [7,31]. The format of this document is as follows: The Hopf bifurcation criteria and the temporal model we employ are provided in Section 2, while the spatial-temporal model and the Turing instability requirements are covered in Section 3. The numerical findings are shown in Section 5, while the linear amplitude equations for the spiral and target patterns are inferred in Section 4. Section 6 concludes with a conclusion of the work that has been done thus far.

## 2. The Model

In many ecological contexts, the original Lotka-Volterra model created to comprehend fundamental prey-predator interactions is being utilised better to understand complicated prey-predator dynamics [33]. We use Bazykin's modified Lotka-Volterra model and an extension of the traditional Rosenzweig-McArthur model [7,31] as our temporal system. Predators' mortality rate and the logistic growth of their prey are controlled by the Holling type III response function, which the Bazykin model implies. An element of predator interference is incorporated into the model [31] to address intra-specific rivalry among the predators, which raises their mortality rates and consequently reduces the adequate predation pressure. At any given time t, the densities of the prey and predator populations are denoted by the variables $N(t)$ and $P(t)$. Following are the ordinary differential equations that result from applying the

assumptions of Bazykin's model:

$$\begin{aligned} \frac{dN}{dT} &= k_1 N(1-\frac{N}{N_0}) - \frac{k_3 NP}{k_2+N^2}, \\ \frac{dP}{dT} &= \frac{\gamma k_3 NP}{k_2+N^2} - k_4 P - k_5 P^2, \end{aligned} \tag{2.1}$$

under the initial assumptions that $N(0) \geq 0, P(0) \geq 0$. A distortion is introduced into the response function in this instance to stop the predator from expanding exponentially. Here, the rates of food replenishment are denoted by $k_1$, the prey's carrying capacity by $N_0$, the satiation constant by $k_2$, and the predator reproduction rate by $k_3$. Furthermore, $\gamma$ represents the specialist predator's conversion efficiency, $k_4$ represents the death rate of predators, and $k_5$ represents the predator's interaction. Choosing $t = \frac{k_1}{\rho}T$, $x = \frac{a}{k_2}N$, $y = \frac{\rho k_3}{\beta k_1 k_2}P$ we derive Bazykin's model in nondimensional space as,

$$\begin{aligned} \frac{dx}{dt} &= \rho x(1-\frac{x}{k}) - \frac{\beta xy}{1+\frac{x^2}{\alpha}}, \\ \frac{dy}{dt} &= \mu(\frac{\gamma xy}{1+\frac{x^2}{\alpha}} - y - \xi y^2), \end{aligned} \tag{2.2}$$

where

$$k = \frac{N_0}{k_2}, \alpha = \frac{a}{k_2}, \mu = \frac{\beta k_2}{k_1 k_3}, \gamma = \frac{\beta k_1^2 k_2}{\rho}, \xi = \frac{\beta^2 k_5 k_1^3 k_2^3}{\rho^2 k_3^2}.$$

In this instance, the multiplicative component of $\mu$ is associated with the reaction term in the growth equation for predators. Target and spiral patterns are produced by selecting $\mu$ with the appropriate values.

### 2.1. Steady States

As the equations' positive solutions, the equilibrium solutions of (2.2),

$$\begin{aligned} \rho x(1-\frac{x}{k}) - \frac{\beta xy}{1+\frac{x^2}{\alpha}} &= 0 = f_1(x,y), \\ \mu(\frac{\gamma xy}{1+\frac{x^2}{\alpha}} - y - \xi y^2) &= 0 = f_2(x,y), \end{aligned} \tag{2.3}$$

From (2.3), we obtain the entire extinction state, or trivial solution, $(0,0)$, and the predator extinction state, or $(k,0)$. In the interior of the first quadrant, the points where two non-trivial nullclines meet are the interior steady points. A continuous curve is used to illustrate the non-trivial prey nullcline,

$$\rho(1-\frac{x}{k}) - \frac{\beta y}{1+\frac{x^2}{\alpha}} = 0 \tag{2.4}$$

connecting the positions $(k,0)$ and $(0,\frac{\rho}{\beta})$. Non-trivial predators have a nullcline provided by

$$\frac{\gamma x}{1+\frac{x^2}{\alpha}} - 1 - \xi y = 0 \tag{2.5}$$

The horizontal asymptote $y = \frac{2\xi}{\gamma\alpha \pm \sqrt{\gamma^2 - \frac{4}{\alpha}}}$ bounded above, which is monotonically increasing, intersects the x-axis at $(\frac{\gamma\alpha \pm \sqrt{\gamma^2-\frac{4}{\alpha}}}{2}, 0)$ and stays in the first quadrant for $x \geq \frac{\gamma\alpha \pm \sqrt{\gamma^2-\frac{4}{\alpha}}}{2}$. At least one internal equilibrium point will exist given $\alpha > 1$ and $\frac{\gamma\alpha \pm \sqrt{\gamma^2-\frac{4}{\alpha}}}{2} < k$. This is a geometric fact. Depending on extra parametric limitations, there can be one to three inner equilibrium points; [7,31] provides a detailed explanation on this topic.

A positive root of the fifth-order equation is $x_*$ if $(x_*, y_*)$ is a typical interior steady state of (2.6). Without losing generality, this assumption can given as

$$\frac{\xi\rho}{\beta k\alpha^2}x_*^5 - \frac{\xi\rho}{\beta\alpha^2}x_*^4 + \frac{\xi\rho}{\beta k\alpha}x_*^3 + (\frac{\xi\rho}{\beta k\alpha} - \frac{\xi\rho}{\beta\alpha} - \frac{1}{\alpha})x_*^2 + (\frac{\xi\rho}{\beta k} + \gamma)x_* - (\frac{\xi\rho}{\beta} - 1) = 0 \tag{2.6}$$

$y_*$ is a positive solution that can be derived from (2.3)

$$y_* = \frac{\rho}{\beta}(1 - \frac{x_*}{k})(1 + \frac{x_*^2}{\alpha}) \tag{2.7}$$

We are interested in the parametric domain where the trace is negative, and the determinant of the Jacobian matrix is optimistic, provided that the Turing instability condition is satisfied for the interior equilibrium point.

### 2.2. Hopf Bifurcation

The bifurcation case is only the persisting steady point $(x_*, y_*)$. When a complex conjugate pair with zero fundamental components makes up the eigenvalues of the linearised system at a fixed point, a Hopf bifurcation occurs. To evaluate the Jacobian of the system at the fixed point, J, a zero trace at the Hopf bifurcation point is necessary. We find that for the solution of coexistence $(x_*, y_*)$,

$$J = \begin{bmatrix} j_{11} & j_{12} \\ j_{21} & j_{22} \end{bmatrix},$$

where

$$\begin{aligned} j_{11} &= \rho - \frac{2\rho x}{k} - \frac{\beta y(1 - \frac{x^2}{\alpha})}{(1 + \frac{x^2}{\alpha})^2}, j_{12} = -\frac{\beta x}{1 + \frac{x^2}{\alpha}} \\ j_{21} &= \frac{\beta y(1 - \frac{x^2}{\alpha})}{(1 + \frac{x^2}{\alpha})^2}, j_{22} = \frac{\mu\gamma x}{1 + \frac{x^2}{\alpha}} - \mu - 2\mu\xi y. \end{aligned}$$

For the model (2), we consider $\mu$ the bifurcation parameter. Assume that J's eigenvalues are $\lambda(\mu), \bar{\lambda}(\mu) = \lambda_1(\mu) \pm \iota\lambda_2(\mu)$. Consequently, Hopf bifurcation happens at $\mu = \mu_0$ if

$$\lambda_1(\mu_0) = 0, \lambda_2(\mu_0) \neq 0 \quad and \quad \frac{d}{d\mu}\lambda_1(\mu_0) \neq 0.$$

The threshold for Hopf bifurcation is determined by

$$j_{11} + j_{22} = 0,$$

i.e

$$\mu = \frac{(\rho - \frac{2\rho x}{k})\gamma^2x^2 - \beta y(1 - \frac{x^2}{\alpha})(1 + \xi y)^2}{\xi\gamma^2x^2y}.$$

Similarly

$$\begin{aligned} \beta &= \frac{(\rho - \frac{2\rho x}{k})\gamma^2x^2 - \mu\xi\gamma^2x^2y}{y(1 - \frac{x^2}{\alpha})(1 + \xi y)^2}, \alpha = \frac{\beta x^2y(1 + \xi y)^2}{(\mu\xi\gamma^2x^2y - \rho - \frac{2\rho x}{k})\gamma^2x^2 + \beta y(1 + \xi y)^2}, \\ \rho &= \frac{\mu\xi\gamma^2x^2y + \beta y(1 - \frac{x^2}{\alpha})(1 + \xi y)^2}{(1 - \frac{2x}{k})\gamma^2x^2}, k = \frac{2\gamma^2\rho x^3}{\gamma^2x^2\rho - \mu\xi\gamma^2x^2y + \beta y(1 - \frac{x^2}{\alpha})(1 + \xi y)^2} \\ \gamma &= \frac{\sqrt{\beta y(1 - \frac{x^2}{\alpha})}(1 + \xi y)}{\sqrt{(\rho - \frac{2\rho x}{k})x^2} - \mu\xi x^2y}, \\ \xi &= -\frac{-(2y + \frac{\gamma^2\mu x^2}{\beta}(1 - \frac{x^2}{\alpha})) \pm \sqrt{(2y + \frac{\gamma^2\mu x^2}{\beta}(1 - \frac{x^2}{\alpha}))^2 - 4y(1 - \frac{(\rho - \frac{2\rho x}{k})\gamma^2x^2}{\beta y(1 - \frac{x^2}{\alpha})})}}{2y}. \end{aligned}$$

The condition mentioned above explicitly yields the crucial value $\mu_0$. In Figure (5), we have displayed the Hopf bifurcation curve about the parameter $\mu$.
Figures (1) to (7) demonstrate the bifurcation diagram and Hopf bifurcation diagram with parametric values $\rho = 0.169, k = 1.569, \beta = 0.81, \alpha = 0.358, \mu = 0.23, \xi = 0.91, \gamma = 5.821$ and using the steady point $(0.2353341535, 0.2047832727)$.
(i) From Figure (1) to (7) in the bifurcation diagram, the points H, BP, BT, GH, LP, CP, and LPC are defined as Hopf point, branch point, Bogdanov-taken, generalized Hopf, limit point, cusp point, and limit point cycle respectively.
(ii)From Figures (1) to (7) in the bifurcation diagram, black, green, blue, and magenta are defined as stable EP, unstable EP, limit point curve, and Hopf curve, respectively.
(iii) From Figures (1) to (7) in the periodic Hopf bifurcation diagram, green, blue, and red are defined as stable Hopf, unstable Hopf, and limit point cycle, respectively.
(iv)From Figures (2), (4), (5), and (7) in the Hopf bifurcation diagram, it is transferred as unstable to stable through LPC, and green and blue portions indicate the stable and unstable of the Hopf Bifurcation.
(vi) In Figure (3), plotting between the prey-predator population with parameter $\gamma$, the bifurcation diagram does not get any Hopf point; it indicates that the system does not get a Hopf bifurcation diagram.

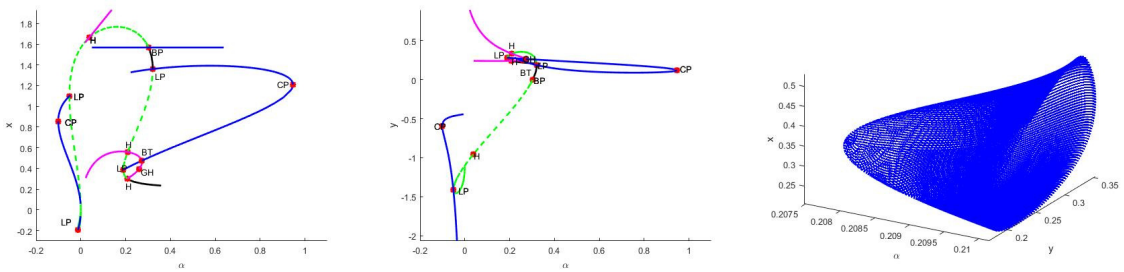


Figure 1: The bifurcation and Hopf bifurcation diagram represents between the $x$, $y$, and $\alpha$ planes.

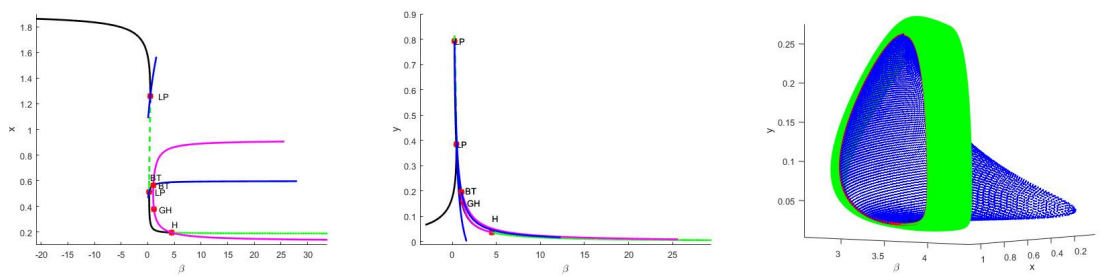


Figure 2: The bifurcation and Hopf bifurcation diagram represents between the $x$, $y$, and $\beta$ planes.

## 3. Spatio-Temporal Model

A restricted domain $\Omega \in R^2$ with a closed boundary $\partial\Omega$ is considered. For the prey and predator populations, let $x(x_1, y_1, t)$ represent the nondimensional population densities at point $x(x_1, y_1) \in \Omega$ and time t, respectively. The following coupled reaction-diffusion equations about the dimensionless variables define the spatiotemporal model, which is comparable to the temporal Bazykin's model (2.2),

$$\begin{aligned} \frac{\partial x}{\partial t} &= \rho x(1 - \frac{x}{k}) - \frac{\beta xy}{1 + \frac{x^2}{\alpha}} + \Delta^2 x, \\ \frac{\partial y}{\partial t} &= \mu(\frac{\gamma xy}{1 + \frac{x^2}{\alpha}} - y - \xi y^2) + D\Delta^2 y, \end{aligned} \tag{3.1}$$

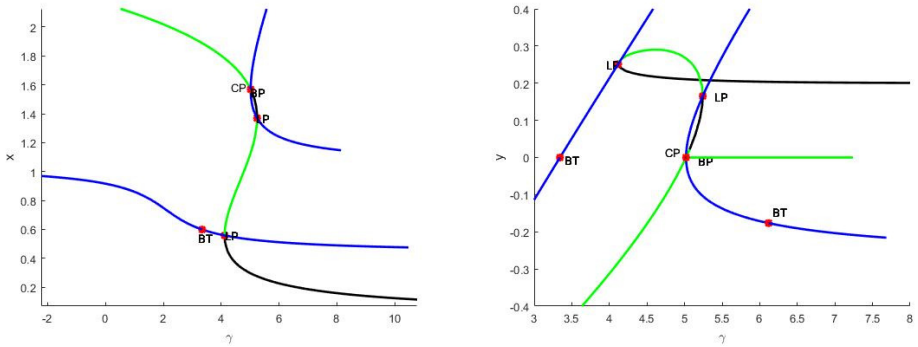


Figure 3: The bifurcation diagram represents the $x$, $y$, and $\gamma$ planes.

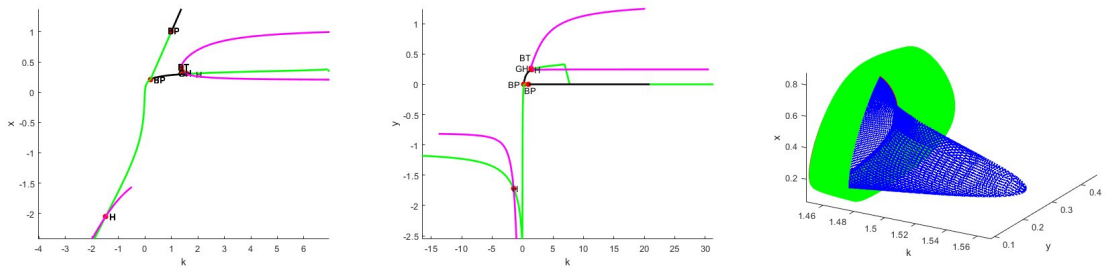


Figure 4: The bifurcation and Hopf bifurcation diagram represents between the $x$, $y$, and $k$ planes.

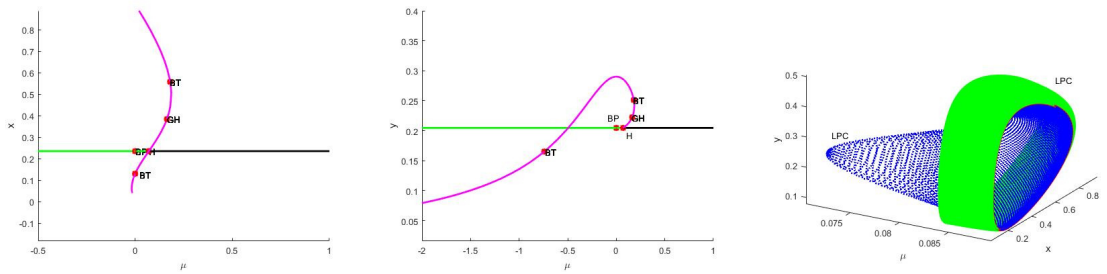


Figure 5: The bifurcation and Hopf bifurcation diagram represents between the $x$, $y$, and $\mu$ planes.

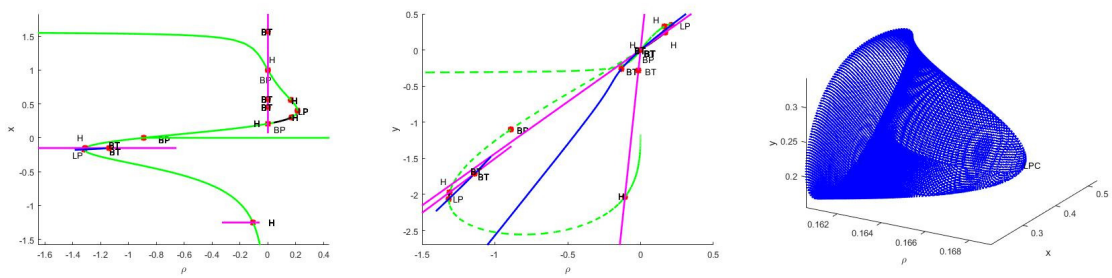


Figure 6: The bifurcation and Hopf bifurcation diagram represents between the $x$, $y$, and $\rho$ planes.

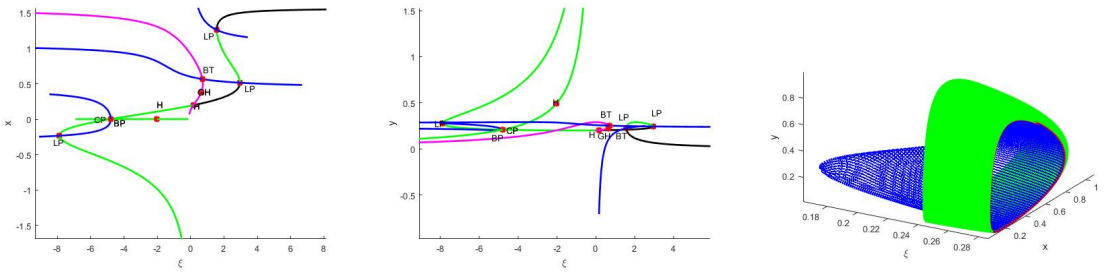


Figure 7: The bifurcation and Hopf bifurcation diagram represents between the $x$, $y$, and $\xi$ planes.

where $\Delta^2$ is the two-dimensional Laplacian operator, and D is the predators' diffusivity coefficients ratio to the prey's. The nonnegative initial conditions apply to these equations, and the no-flux border is,

$$\begin{aligned} \frac{\partial x}{\partial v} &= \frac{\partial y}{\partial v} = 0, (x_1, y_1) \in \partial\Omega, t \geq 0, \\ x(x_1, y_1, t) &\geq 0, y(x_1, y_1, t) \geq 0, (x_1, y_1) \in \Omega \end{aligned} \tag{3.2}$$

where the derivative to $\partial\Omega$ along the unit normal vector is indicated by $\frac{\partial}{\partial v}$.

### 3.1. Turing Instability

As defined by [33] and [39], Turing instability occurs when a heterogeneous shock of moderate magnitude causes a stable homogeneous steady-state to become unstable. Since they meet the equations, we consider $x(x_1, y_1, t) \cong x_*$ and $y(x_1, y_1, t) \cong y_*$ to be the homogeneous stable states for (3.1). For the temporal model, the homogeneous steady is locally asymptotically stable. Therefore, we need a negative trace and a positive determinant. The linear stability analysis of the spatiotemporal model (3.1) around the homogeneous, stable state $(x_*, y_*)$ yields the following requirements for the Turing instability [33],

$$\begin{aligned} j_{11} + j_{22} &\leq 0, \\ j_{11}j_{22} - j_{21}j_{12} &\geq 0, \\ Dj_{11} + j_{22} &\geq 2\sqrt{D(j_{11}j_{22} - j_{21}j_{12})}, \end{aligned}$$

additionally, the Turing bifurcation curve equation is supplied by

$$Dj_{11} + j_{22} = 2\sqrt{D(j_{11}j_{22} - j_{21}j_{12})}. \tag{3.3}$$

Previous finds of Turing patterns include spot, labyrinthine, chaotic, quasiperiodic, mixing of spots and stripes, and localised structures [6,31], by spatiotemporal Bazykin's model. The present study uses a theoretical framework based on linear amplitude equations to determine the parameter values leading to the formation of spiral patterns and better understand the mechanisms behind their formation.

## 4. Derivation of Amplitude Equations for the Spiral and Target Patterns

We perform the multi-scale analysis [16,17,35] to derive the proper amplitude equation for spiral and target patterns. In compact form, the coupled reaction-diffusion equations are expressed as

$$\begin{aligned} \frac{\partial x}{\partial t} &= f_1(x, y) + \Delta^2 x, \\ \frac{\partial y}{\partial t} &= \mu f_2(x, y) + D\Delta^2 y, \end{aligned} \tag{4.1}$$

where,

$$\begin{aligned} f_1(x, y) &= \rho x(1 - \frac{x}{k}) - \frac{\beta xy}{1 + \frac{x^2}{\alpha}}, \\ f_2(x, y) &= \frac{\gamma xy}{1 + \frac{x^2}{\alpha}} - y - \xi y^2, \end{aligned} \tag{4.2}$$

We assign $u = x - x_*$ and $v = y - y_*$ to linearise (4.1) concerning the homogeneous stable state $(x_*, y_*)$. The second and higher order components don't matter because they are minor perturbation terms, $u \cong u(x_1, y_1, t)$ and $v \cong v(x_1, y_1, t)$. Consequently, the linearised equations become,

$$\begin{aligned} \frac{\partial u}{\partial t} &= a_{11}u + a_{12}v + \Delta^2 u, \\ \frac{\partial v}{\partial t} &= \mu a_{21}u + \mu a_{22}v + D\Delta^2 v, \end{aligned} \tag{4.3}$$

where $a_{11} = \frac{\partial f_1}{\partial x}_{(x_*,y_*)}$, $a_{12} = \frac{\partial f_1}{\partial y}_{(x_*,y_*)}$, $a_{21} = \frac{\partial f_2}{\partial x}_{(x_*,y_*)}$, $a_{22} = \frac{\partial f_2}{\partial y}_{(x_*,y_*)}$.
Given that $\mu_0$ is the value at which the Hopf bifurcation occurs for $\mu$, $\mu_0$ meets the following condition: $\mu_0 a_{22} + a_{11} = 0$. Close to the Hopf bifurcation threshold, the control parameter can be adjusted as $\mu = \mu_0 + \epsilon\mu_1$ for both the spiral and the goal wave solution, where $0 \leq \epsilon \ll 1$. The choice could be more remarkable. The two-dimensional polar coordinates are defined as $r = r_0 + \epsilon r_1$ and $\theta = \theta_0 + \sqrt{\epsilon}\theta_1$. Once the scalar variables have been expanded, we express the time variable as $t = t_0 + \epsilon\tau$ as,

$$\begin{aligned} u &= \epsilon u_1 + \epsilon^2 u_2 + ..., \\ v &= \epsilon v_1 + \epsilon^2 v_2 + .... \end{aligned} \tag{4.4}$$

Using (4.3), we get when we enter these expressions:

$$\begin{aligned} \epsilon(\frac{\partial u_1}{\partial t_0} - a_{11}u_1 - a_{12}v_1 - \Delta_0^2 u_1) + \epsilon^2(\frac{\partial u_2}{\partial t_0} \quad + \\ \frac{\partial u_1}{\partial \tau} - a_{11}u_2 - a_{12}v_2 - \Delta_0^2 u_2 - \Delta_\epsilon^2 u_1) + ... \quad &= \quad 0, \end{aligned} \tag{4.5}$$

$$\begin{aligned} \epsilon(\frac{\partial v_1}{\partial t_0} - \mu_0 a_{11}u_1 - \mu_0 a_{22}v_1 - D\Delta_0^2 u_1) + \epsilon^2(\frac{\partial v_2}{\partial t_0} + \frac{\partial v_1}{\partial \tau} \quad - \\ \mu_1 a_{11}u_1 - \mu_1 a_{22}v_1 - \mu_0 a_{21}u_2 - \mu_0 a_{22}v_2 - \Delta_0^2 v_2 - \Delta_\epsilon^2 v_1) + ... \quad &= \quad 0, \end{aligned} \tag{4.6}$$

where,

$$\Delta_0^2 \equiv \frac{1}{r_0}\frac{\partial}{\partial r_0} r_0 \frac{\partial}{\partial r_0} + \frac{1}{r_0^2}\frac{\partial^2}{\partial \theta_0^2}, \Delta_\epsilon^2 \equiv \frac{1}{r_0}\frac{\partial}{\partial r_0} r_0 \frac{\partial}{\partial r_1} + \frac{1}{r_0^2}\frac{\partial^2}{\partial \theta_1^2}$$

Taking the $O(\epsilon)$ terms from equations (4.5) and (4.6), we obtain

$$\begin{bmatrix} 0 \\ 0 \end{bmatrix} = \begin{bmatrix} \frac{\partial}{\partial t_0} - \Delta_0^2 - a_{11} & -a_{12} \\ -mu_0 a_{21} & \frac{\partial}{\partial t_0} - D\Delta_0^2 - \mu_0 a_{22} \end{bmatrix} = L \begin{bmatrix} u_1 \\ v_1 \end{bmatrix}. \tag{4.7}$$

Due to the common observation of spirals and targets near the Hopf bifurcation threshold, the following trial solutions are assumed:

$$\begin{bmatrix} u_1 \\ v_1 \end{bmatrix} = A(r_1, \theta_1, \tau) \begin{bmatrix} \hat{u_1} \\ \hat{v_1} \end{bmatrix} e^{\alpha t_0}, \tag{4.8}$$

Hence, under zero diffusion conditions, $\alpha$ can be found using equation (4.7). Therefore, $\alpha$ represents the operator's eigenvalue.

$$L_0 = \begin{bmatrix} \frac{\partial}{\partial t_0} - a_{11} & -a_{12} \\ -mu_0 a_{21} & \frac{\partial}{\partial t_0} - \mu_0 a_{22} \end{bmatrix}$$

and the pair of $L_0$ eigenvalues is provided by

$$\alpha_{1,2} = \frac{(\mu_0 a_{22} + a_{11}) \pm \sqrt{(\mu_0 a_{22} + a_{11})^2 - 4\mu_0(a_{22}a_{11} - a_{21}a_{12})}}{2}. \tag{4.9}$$

We will choose $\alpha = \alpha_2$ for convenience even though $\alpha_1$ and $\alpha_2$ can be used in the calculations. $\mu_0 = \frac{-a_{11}}{a_{22}}$ is the outcome of $\alpha$ turning completely imaginary at the Hopf bifurcation threshold. Next, $\omega_H = \sqrt{\mu_0(a_{22}a_{11} - a_{21}a_{12})}$ yields the Hopf frequency. The explicit solutions of $u_1$ and $v_1$ are obtained by substituting the trial solution (4.8) into equation (4.7). The answer for $u_1$ and $v_1$ are as follows. This yields $\frac{\hat{u_1}}{\hat{v_1}} = \frac{a_{12}}{\alpha - a_{11}}$.

$$u_1 = A(r_1, \theta_1, \tau)a_{12}e^{\alpha t_0} + c.c., \tag{4.10a}$$
$$v_1 = A(r_1, \theta_1, \tau)(\alpha - a_{11})e^{\alpha t_0} + c.c., \tag{4.10b}$$

in which the phrase's complex conjugate before is indicated by c.c. After that, by gathering the $O(\epsilon^2)$ terms from (4.5) and (4.6), we obtain

$$L\begin{bmatrix} u_2 \\ v_2 \end{bmatrix} = \begin{bmatrix} \frac{\partial}{\partial \tau} + \Delta_\epsilon^2 & 0 \\ -mu_1a_{21} & -\frac{\partial}{\partial \tau} + D\Delta_\epsilon^2 + \mu_1 a_{22} \end{bmatrix} \begin{bmatrix} u_1 \\ v_1 \end{bmatrix}. \tag{4.11}$$

Terms such as $\frac{1}{r_0}\frac{\partial}{\partial r_0}r_0\frac{\partial}{\partial r_0}$ do not need to be considered. As the intensity of $u_1$ and $v_1$ is independent of $r_0$, and $\frac{1}{r_0}\frac{\partial}{\partial r_0}r_0\frac{\partial}{\partial r_1}$ occur in the $O(\epsilon)$ evolution of the Laplacian. The expression $L_0$ acting on $u_1$ and $v_1$ has an eigenvalue of zero. Hence, a solvability condition must be applied to solve equation (4.11). Consequently, Ghosh and Ray state that the zero eigenvalue $L_0$ is represented by the left eigenvector, of which the right side of equation (4.11) must be orthogonal to it [16]. The complex conjugate is represented by the symbol $*$, and this left eigenvector is proportional to $(u_1^*, v_1^*)$. Consequently,

$$(u_1^* v_1^*)\begin{bmatrix} \frac{\partial}{\partial \tau} + \Delta_\epsilon^2 & 0 \\ -mu_1a_{21} & -\frac{\partial}{\partial \tau} + D\Delta_\epsilon^2 + \mu_1 a_{22} \end{bmatrix} \begin{bmatrix} u_1 \\ v_1 \end{bmatrix} = 0. \tag{4.12}$$

We can replace (4.10) with it to obtain this solvability condition as,

$$\frac{\partial A}{\partial \tau} = \frac{a_{12}^2 + D(a_{11}^2 + \omega_H^2)}{a_{12}^2 + a_{11}^2 + \omega_H^2}\Delta_\epsilon^2 A + \frac{\mu(a_{22}(a_{11}^2 + \omega_H^2) - a_{21}a_{11}a_{12})}{a_{12}^2 + a_{11}^2 + \omega_H^2}A + \frac{\mu_1\omega_H a_{21}a_{12}}{a_{12}^2 + a_{11}^2 + \omega_H^2}\iota A, \tag{4.13}$$

where $\alpha = -\iota\omega_H$. Ultimately, the required amplitude equation, after converting to the original scale, is

$$\frac{\partial A}{\partial t} = \frac{B_1}{r}\frac{\partial A}{\partial r} + \frac{C_1}{r^2}\frac{\partial^2 A}{\partial r^2} + \epsilon\mu_1 B_2 A + \iota\epsilon\mu_1 B_3 A, \tag{4.14}$$

where

$$B_1 = \frac{a_{12}^2 + D(a_{11}^2 + \omega_H^2)}{a_{12}^2 + a_{11}^2 + \omega_H^2},$$
$$B_2 = \frac{\mu(a_{22}(a_{11}^2 + \omega_H^2) - a_{21}a_{11}a_{12})}{a_{12}^2 + a_{11}^2 + \omega_H^2},$$
$$B_3 = \frac{\mu_1\omega_H a_{21}a_{12}}{a_{12}^2 + a_{11}^2 + \omega_H^2}.$$

Assuming a general spiral or target solution of the following type [24], we can solve (4.14).

$$A(r, \theta, t) = \hat{A}(r)e^{\iota(\omega t + \phi(r) + m\theta)} \tag{4.15}$$

whose distance from the core is $r$, and whose polar angle is $\theta$. In addition, the spiral type $\phi(r)$, the spatial amplitude $\hat{A}(r)$, and the frequency $\omega$ of a spiral or target wave are also given. One characteristic of spiral defects is the spiral-arm number, also known as the nonzero winding number m, of the phase of any contour surrounding the core. To obtain their determined expressions, the linear amplitude equations for the spiral and target patterns are solved independently in the following two subsections.

### 4.1. Approximated Expression for Spiral

By dividing the real and imaginary components of (4.15) and inserting them into (4.14), we get

$$\frac{B_1 m^2}{r^2} = \frac{B_1}{r\hat{A}}\frac{d\hat{A}}{dr} + \epsilon\mu_1 B_2, \tag{4.16}$$

and

$$\omega = \frac{B_1}{r}\frac{d\hat{\phi}}{dr} + \epsilon\mu_1 B_3, \tag{4.17}$$

Once we compute $\phi$ and $\hat{A}$, we get

$$\hat{A}(r) = C_1 r^{m^2} e^{-(\epsilon\mu_1 B_2)\frac{r^2}{2B_1}}, \tag{4.18a}$$

$$\phi(r) = \frac{\omega - \epsilon\mu_1 B_3}{2B_1} r^2 + C_2, \tag{4.18b}$$

where the integrating constants $C_1$ and $C_2$ are used.

### 4.2. Approximated Expression for Target

Since a target response is axisymmetric, the standard solution for a target is of the type given in (4.15) with $m = 0$. Consequently, we may deduce from equation (4.16) that,

$$\frac{B_1}{r\hat{A}}\frac{d\hat{A}}{dr} + \epsilon\mu_1 B_2 = 0, \tag{4.19}$$

which, once $\hat{A}$ is taken into consideration, yields

$$\hat{A}(r) = C_3 r^{m^2} e^{-(\epsilon\mu_1 B_2)\frac{r^2}{2B_1}} \tag{4.20}$$

when the integration constant $C_3$ is used. Equation (4.17) allows us to determine

$$\phi(r) = \frac{\omega - \epsilon\mu_1 B_3}{2B_1} r^2 + C_4, \tag{4.21}$$

where an integrating constant is denoted by $C_4$.

## 5. Numerical Simulation

Theoretical representations of the spiral and target solutions derived from the corresponding linear amplitude equations have been established. These analytical findings are validated through numerical examples and corroborated by matching numerical simulations. The coupled reaction–diffusion equations with no-flux boundary conditions are numerically solved using a five-point stencil finite-difference scheme for the Laplacian term, combined with a forward Euler method for the temporal integration.

$$\frac{\partial x}{\partial t} = \rho x(1 - \frac{x}{k}) - \frac{\beta xy}{1 + \frac{x^2}{\alpha}} + \Delta^2 x, \tag{5.1}$$

$$\frac{\partial y}{\partial t} = \mu(\frac{\gamma xy}{1 + \frac{x^2}{\alpha}} - y - \xi y^2) + D\Delta^2 y,$$

Two complex roots of (2.6) and a unique non-negative real root are provided by the parameter values $\rho = 0.34, k = 45, \beta = 1.43, \alpha = 1.339, \gamma = 0.110013, \mu = 0.015, and \xi = 0.11201$ in the system (5.1). The patterns can be produced by changing the values of $\mu$ and $D$.

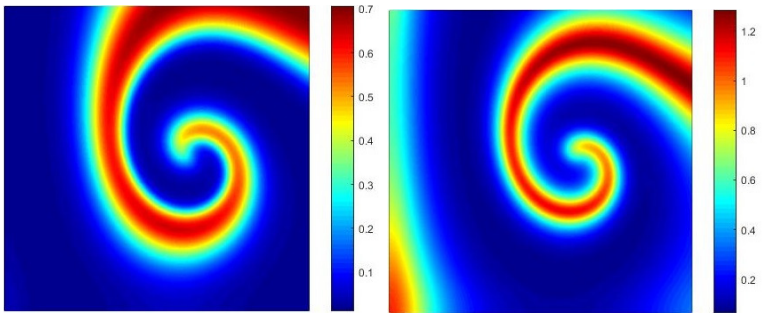


Figure 8: Initial circumstance and parameter values are $\rho = 0.34, k = 45, \beta = 1.43, \alpha = 1.339, \gamma = 0.110013, \mu = 0.5815, \xi = 0.11201$, and $D = 1.3$, as well. Figure (9) displays a computational model of a spiral design.

### 5.1. Result for Spiral Patterns

Using a two-dimensional grid, we set the grid spacing to $\Delta x = \Delta y = 1$ and the time step to $\Delta t = 0.01$. Numerical simulations of spiral patterns involve creating a suitable beginning set of conditions. Such an initial state may be found in the writings of Malchow et al. [30] as well as in subsequent works by writers [32,44]. For specific parameter values, scientists have found a variety of distorted structures, such as interacting spiral chaos, rather than a single spiral pattern. System (5.1) and beginning condition are solved as follows by using boundary conditions (3.2):

$$\begin{aligned} x(x_1, y_1, 0) &= x_* - (1.25 \times 10^{-18})(x - 1600)(y - 800) \\ &- (0.1875 \times 10^{-10})(x - 2)(y - 300), \qquad (5.2a) \\ y(x_1, y_1, 0) &= y_* - (0.3 \times 10^{-8})(x - 1500) - (1.55 \times 10^{-10})(y - 50), \qquad (5.2b) \end{aligned}$$

Gradually, a single spiral pattern emerges, coiling around $t = 800$ and extending throughout the quadratic region. Even with an increased number of iterations, the spiral does not break into any other shape; instead, its tip rotates continuously without changing position. This demonstrates that, as noted in the caption of Fig. (8), the model (5.1) with the chosen set of parameters evolves into a revolving spiral.

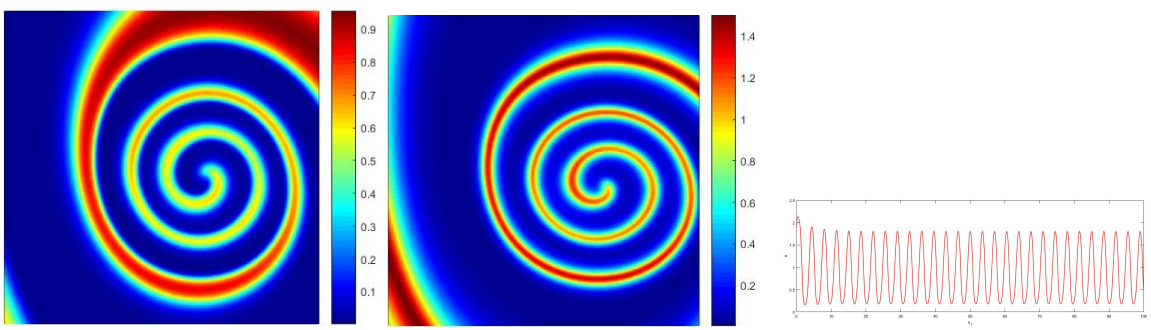


Figure 9: The figure illustrates how the spiral pattern numerical simulation validates the analytical answer. Using the same parameter values as in Figure (8), the approximated analytical solutions $x = x_* + \epsilon\Re(u_1)$ and $y = y_* + \epsilon\Re(u_1)$ are plotted in (a). A numerical simulation of the spiral pattern is then performed using the approximated solution as an initial condition.

## 6. Discussion and Conclusion

This study examines the conditions under which spiral patterns emerge in the spatiotemporal extension of Bazykin's prey–predator model. The governing equations for spiral wave formation have been

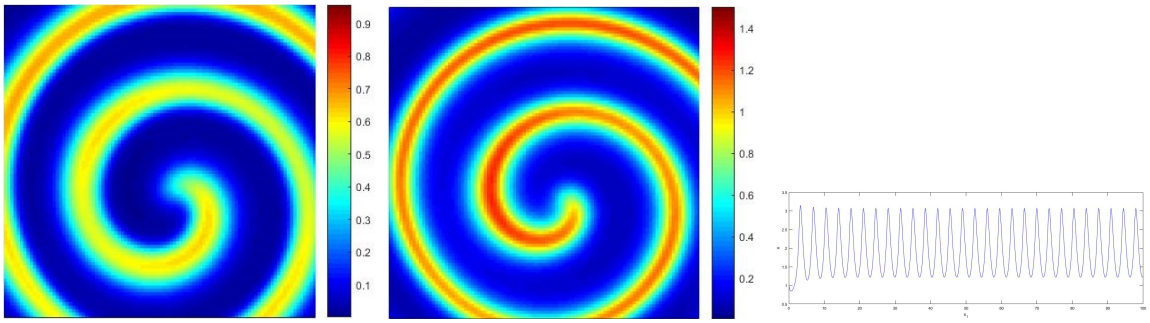


Figure 10: The figure illustrates how the spiral pattern numerical simulation validates the analytical answer. The approximated analytical solution $x = x_* + \epsilon\Re(u_1)$ and $y = y_* + \epsilon\Re(u_1)$ in (a) are plotted using the same parameter values as $\rho = 0.74, k = 42, \beta = 1.43, \alpha = 1.339, \gamma = 0.110013, \mu = 0.5815, \xi = 0.21201$, and $D = 6$.

derived analytically, and numerical simulations confirm that these patterns occur within a specific parametric domain appropriate to Bazykin's framework. Bazykin's model was selected due to its incorporation of predator interference, which leads to more intricate dynamics compared to conventional predator–prey models. Moreover, the temporal subsystem of the model presents analytical challenges, as its interior equilibrium points correspond to the roots of a fifth-order polynomial. In the full spatiotemporal model, which includes three homogeneous steady states, only one is temporally stable. Regardless of the perturbation magnitude, the solution always converges to this stable interior state, preventing pattern formation around the remaining two homogeneous states. Since only one equilibrium satisfies the Turing instability condition, it is difficult to define the appropriate parametric domain directly.

The main objective of this work was to obtain analytical approximations of spiral patterns. To this end, a multiscale perturbation technique was employed to derive a linear amplitude equation based on the linearized form of the spatiotemporal Bazykin model near the coexisting homogeneous steady state. Solutions to this amplitude equation provide explicit analytical expressions for spiral waves. These approximated solutions, when used as initial conditions in numerical simulations of the original nonlinear system, successfully generate spiral patterns. This approach, while previously applied to chemical reaction systems that exhibit spiral behavior [8,16,17,35], has not been widely applied to ecological models of interacting populations. It offers a promising framework for other spatiotemporal models exhibiting similar dynamics.

The nonlinear wave equations that emerge from the weakly nonlinear analysis are generally intractable using exact analytical methods. Thus, obtaining explicit solutions for spiral and target waves remains a challenge. Moreover, in most ecological models studied so far, spiral waves—if they form—tend to collapse into interacting spiral chaos over time [30,32]. Arbitrary perturbations around the homogeneous equilibrium often lead to non-patterned oscillatory behavior, complicating the identification of initial conditions required for sustained spiral formation.

In the current study, the analytical and numerical results show strong agreement. Although only a first-order perturbation analysis was conducted, extending the comparison to higher-order approximations is a goal for future work. Importantly, our findings confirm that the observed spiral patterns are not numerical artifacts, but genuine solutions of the system. This research offers a promising avenue for studying the ecological implications of spiral pattern formation in prey–predator dynamics and may provide insight into spatiotemporal interactions in a variety of ecological settings.

Finally, when the approximate spatial solutions were visualized at specific time snapshots, spiral and target patterns were the only visible structures. These patterns emerged consistently when the approximated solutions were used as initial conditions in the nonlinear model with the corresponding boundary conditions. This approach can be applied to other spatiotemporal systems, especially those with parameters near the Turing–Hopf bifurcation point. It also reduces the uncertainty involved in selecting initial conditions conducive to spiral pattern formation.

## Declaration

The authors declare that there is no conflict of interest and all the numerical simulations were carried out using Maple & MATLAB toolboxes purchased by the Department of Mathematics, Central University of Odisha, and that all the data are available upon request, subject to ethical considerations and at the discretion of the authors.

## References


1. Aslanidi, O.V., Clayton, R.H., Holden, A.V., Phillips, H.K., Ward, R.J., *Vulnerability to reentry, and drift, stability and breakdown of spiral waves in a linear gradient of GK in a Luo-Rudy 1 virtual ventricular tissue*, International Journal of Bifurcation and Chaos, 13, 3865–3871, (2003).
2. Barkley, D., *Linear stability analysis of rotating spiral waves in excitable media*, Physical Review Letters, 68, 2090–2093, (1992).
3. Baurmann, M., Gross, T., Feudel, U., *Instabilities in spatially extended predator-prey systems: Spatio-temporal patterns in the neighbourhood of Turing-Hopf bifurcations*, Journal of Theoretical Biology, 245, 220–229, (2007).
4. Banerjee, M., Abbas, S., *Existence and non-existence of spatial patterns in a ratio-dependent predator-prey model*, Ecological Complexity, 21, 199–214, (2015).
5. Banerjee, M., Pterovskii, S., *Self-organized spatial patterns and chaos in a ratio-dependent predator-prey system*, Theoretical Ecology, 4, 37–53, (2011).
6. Banerjee, M., Zhang, L., *Influence of discrete delay on pattern formation in a ratio-dependent prey-predator model*, Chaos, Solitons and Fractals, 67, 73–81, (2014).
7. Bazykin, A.D., *Nonlinear Dynamics of Interacting Populations*, World Scientific Publishing Co. Pvt. Ltd., Singapore, (1998).
8. Bhattacharyay, A., *Spirals and targets in reaction diffusion systems*, Physical Review E, 64, 016113, (2001).
9. Biktasheva, I.V., Holden, A.V., Biktashev, V.N., *Localization of response functions of spiral waves in the Fitzhugh-Nagumo system*, International Journal of Bifurcation and Chaos, 16, 1547–1555, (2006).
10. Bugrim, A.E., Dolnik, M., Zhabotinsky, A.M., Epstein, I.R., *Heterogeneous sources of target patterns in reaction-diffusion systems*, International Journal of Bifurcation and Chaos, 14, 3363–3375, (1996).
11. Cassia-Moura, R., Xie, F., Cerdeira, H.A., *Effect of heterogeneity on spiral wave dynamics in simulated cardiac tissue*, The Journal of Physical Chemistry, 100, 19017–19022, (2004).
12. Cohen, D.S., Neu, J.C., Rosales, R.R., *Rotating spiral wave solutions of reaction-diffusion equations*, SIAM Journal on Applied Mathematics, 35, 536–547, (1978).
13. Cross, M.C., Hohenberg, P.C., *Pattern formation outside of equilibrium*, Reviews of Modern Physics, 65, 851–1112, (1993).
14. Duffy, M.R., Britton, N.F., Murray, J.D., *Spiral wave solutions of practical reaction-diffusion systems*, SIAM Journal on Applied Mathematics, 39, 8–13, (1980).
15. Gambino, G., Lombardo, M.C., Sammartino, M., Sciacca, V., *Turing pattern formation in the Brusselator system with nonlinear diffusion*, Physical Review E, 88, 042925, (2013).
16. Ghosh, P., Ray, D.S., *Amplitude equations for breathing spiral waves in a forced reaction-diffusion system*, The Journal of Chemical Physics, 135, 104112, (2011).
17. Ghosh, S., Ray, D.S., *Selecting spatio-temporal patterns by substrate injection in a reaction-diffusion system*, The European Physical Journal B, 99, 1–7, (2015).
18. Gil, L., Emilsson, K., Oppo, G.-L., *Dynamics of spiral waves in a spatially inhomogeneous Hopf bifurcation*, Physical Review A, 45, (2), (1992).
19. Gong, Y., Christini, D.J., *Antispiral waves in reaction-diffusion systems*, Physical Review Letters, 90, 088302, (2003).
20. Greenberg, J.M., *Spiral waves for $\lambda - \Omega$ systems*, SIAM Journal on Applied Mathematics, 39, 301–309, (1980).
21. Gurney, W.S.C., Veitch, A.R., Cruickshank, I., McGeachin, G., *Circles and spirals: Population persistence in a spatially explicit predator-prey model*, Ecology, 79, 2516–2530, (1998).
22. Hagan, P.S., *Target patterns in reaction-diffusion equations*, Advances in Applied Mathematics, 2, 400–416, (1981).
23. Hagan, P.S., *Spiral waves in reaction-diffusion equations*, SIAM Journal on Applied Mathematics, 4, 762–786, (1982).
24. Ipsen, M., Kramer, L., Sørensen, P.G., *Amplitude equations for description of chemical reaction-diffusion systems*, Physics Reports, 337, 193–235, (2000).

25. Kopell, N., Howard, L.N., *Target pattern and spiral solutions to reaction-diffusion equations with more than one space dimension*, Advances in Applied Mathematics, 2, 417–449, (1981).

26. Kuramoto, Y., Koga, S., *Turbulized rotating chemical waves*, Progress of Theoretical Physics, 3, 1081–1085, (1981).

27. Kuramoto, Y., Yamada, T., *Pattern formation in oscillatory chemical reactions*, Progress of Theoretical Physics, 56, 724–740, (1976).

28. Kuznetsov, Y.A., *Elements of Applied Bifurcation Theory*, Springer, New York, (1998).

29. Li, Z., Gao, M., Hui, C., Han, X., Shi, H., *Impact of predator pursuit and prey evasion on synchrony and spatial patterns in metapopulation*, Ecological Modelling, 185, 245–254, (2005).

30. Malchow, H., Radtke, B., Kallache, M., Medvinsky, A.B., Tikhonov, D.A., Petrovskii, S.V., *Spatiotemporal pattern formation in coupled models of plankton dynamics and fish school motion*, Nonlinear Analysis, 1, 53–67, (2000).

31. Mcgehee, E.A., Schutt, N., Vasquez, D.A., Peacock-Lopez, *Bifurcations, and temporal and spatial patterns of a modified Lotka-Volterra model*, International Journal of Bifurcation and Chaos, 18, 2223–2248, (2008).

32. Medvinsky, A.B., Petrovskii, S.V., Tikhonova, I.A., Malchow, H., Li, B.L., *Spatiotemporal complexity of plankton and fish dynamics*, SIAM Review, 44, 311–370, (2002).

33. Murray, J.D., *Mathematical Biology*, Springer, Heidelberg, (1989).

34. Nikolaev, E.V., Biktashev, V.N., Holden, A.V., *On bifurcations of spiral waves in the plane*, International Journal of Bifurcation and Chaos, 9, 1501–1516, (1999).

35. Riaz, S.S., Ray, D.S., *Spiral pattern in chlorite-iodide-malonic acid reaction: A theoretical and numerical study*, The Journal of Chemical Physics, 123, 174506, (2005).

36. Sheratt, J.A., Lambin, X., Sheratt, T.N., *The effects of the size and shape of landscape features on the formation of traveling waves in cyclic populations*, The American Naturalist, 162, 503–513, (2003).

37. Smith, M.J., Sheratt, J.A., Armstrong, N.J., *The effects of obstacle size on periodic travelling waves in oscillatory reaction-diffusion equations*, Proceedings of the Royal Society A, 464, 365–390, (2008).

38. Steinbock, O., Muller, S.C., *Multiarmed spirals in a light controlled excitable reaction*, International Journal of Bifurcation and Chaos, 3, 437–443, (1993).

39. Turing, A.M., *The chemical basis of morphogenesis*, Philosophical Transactions of the Royal Society of London B, 237, 37–72, (1952).

40. Tyson, J.J., *Singular perturbation theory of target patterns in the Belousov-Zhabotinskii reaction*, Journal de Chimie Physique, 84, 1359–2237, (1987).

41. Tyson, J.J., Keener, J.P., *Singular perturbation theory of traveling waves in excitable media (A Review)*, Physica D, 32, 327–361, (1988).

42. Tyson, J.J., Alexander, K.A., Manoranjan, V.S., Murray, J.D., *Spiral waves of cyclic AMP in a model of slime mold aggregation*, Physica D, 34, 193–207, (1989).

43. Volpert, V., *Elliptic Partial Differential Equations*, Birkhäuser, Basel, (2011).

44. Wang, W., Liu, Q., Jin, Z., *Spatiotemporal complexity of a ratio-dependent predator-prey system*, Physical Review E, 75, 051913, (2007).

45. Wang, W., Zhang, L., Wang, H., Li, Z., *Pattern formation of a prey-predator system with Ivlev-type functional response*, Ecological Modelling, 221, 131–140, (2010).

46. Winfree, A.T., *Spiral waves of chemical activity*, Science, 175, 634–636, (1972).

47. Yamada, T., Kuramoto, Y., *Spiral waves in a nonlinear-dissipative system*, Progress of Theoretical Physics, 55, 2035–2036, (1976).

48. Zaritski, R.M., Ju, J., Ashkenazi, I., *Spontaneous formation of multiarmed spiral waves in various simple models of weakly excitable media*, International Journal of Bifurcation and Chaos, 15, 4087–4094, (2005).

49. Zhou, L.Q., Quyang, Q., *Spiral instabilities in a Reaction-Diffusion System*, The Journal of Physical Chemistry A, 105, 112–118, (2001).

*Atish Kumar Sethy,*
*Department of Mathematics,*
*Central University of Odisha, Koraput,*
*India.*
*E-mail address:* atish_phd@cuo.ac.in

*and*

*Jyotiska Datta (Corresponding Author),*
*Department of Mathematics,*
*Central University of Odisha, Koraput,*
*India.*
*E-mail address:* jyotiska.datta@gmail.com